J Comput Neurosci
DOI 10.1007/s10827-009-0141-y

The cost of linearization

Danielle Morel · William B Levy

Received: 8 May 2008 / Revised: 15 October 2008 / Accepted: 2 February 2009

Abstract Linear additivity of synaptic input is a pervasive assumption in computational neuroscience, and previously Bernander et al. (*Journal of Neurophysiology* 72:2743–2753, 1994) point out that the sublinear additivity of a passive neuronal model can be linearized with voltage-dependent currents. Here we re-examine this perspective in light of more recent findings and issues. Based on *in vivo* intracellular recordings, three voltage-dependent conductances seem to be of interest for pyramidal cells of the forebrain: two of them are amplifying, I_{NaP} and I_h; and one of them is attenuating, I_A. Based on particular I-V characteristics reported in the literature, each of these three voltage-dependent currents linearizes a particular range of synaptic excitation. Computational simulations use a steady-state, one-compartment model. They establish maximal linear ranges, where supralinear effects—due to adding too much of any one conductance—limit these ranges. Specific, carefully selected pairwise combinations of these currents can linearize larger ranges than either current alone. In terms of parameters, the steady-state I-V characteristics of each current are critical. On the other hand, the relationships between the results here and resting conductance to ground, synaptic conductance, and number of active synapses are simple and easily scaled; thus in regard to these three latter dependences, the results here are easily generalized. Finally, to improve our understanding of evolved function, the relative metabolic costs of linearization are quantified. In one case, there is a clear preference arising from this cost consideration (a particular I_h, I_{NaP} pairing is less costly compared to a particular I_A, I_{NaP} pairing that produces an equivalent, linearized range). However in other cases, a preference will depend on the required range; but in any event, the largest linearized range observed here (28 mV), from a combination of I_h and I_A, is significantly more costly than the 20 mV range that the I_h, I_{NaP} pair produces.

Keywords Dendrite · Linearization · Voltage dependent conductances · Metabolic cost · Persistent sodium current · A-type potassium current · Hyperpolarization-activated mixed cation current

Action Editor: Erik De Schutter

D. Morel
Department of Physics and Astronomy,
James Madison University,
Harrisonburg, VA 22807, USA

D. Morel
Physics Department, Stetson University,
DeLand, FL 32723, USA
e-mail: dmorel@stetson.edu

W. B Levy (✉)
Departments of Neurosurgery and of Psychology,
University of Virginia,
Charlottesville, VA 22908, USA
e-mail: wbl@virginia.edu

1 Introduction

Dendritic interactions play a key role in defining the computations performed by a neuron. Judging from the variety of dendritic morphologies and the diversity of voltage-dependent channels with various dendritic localizations, dendrites would seem to perform a variety of computations (e.g., Polsky et al. 2004; Cook et al. 2007; London and Häusser 2005). Among this variety, the linear computation is of particular significance from at least three perspectives.

A linear computation is simplest (McCulloch and Pitts 1943), and therefore of immediate appeal in theoretical and teaching contexts. Second, as pointed out by Levy and Morel (2006), in the context of Bayesian statistical

Published online: 03 April 2009

inferences, linear summation can be optimal. That is, we argue that a neuron, in adding up its inputs, can be considered as performing Bayesian inference (Bernardo and Smith 2000) where the summed input is a summary statistic of a distal event (Levy et al. 1990). Furthermore, only linear summation is allowed when forming a complete and sufficient statistic of fixed dimension, and such sufficient statistics are, by definition, the only information-optimal summary statistic. Beyond such theoretical interests is a third, empirical perspective: some slightly higher order physiological processes have been shown to exhibit linear summation. These include direction-selectivity in simple cells of the cat visual cortex (e.g., DeAngelis et al. 1993; Jagadeesh et al. 1993; Ferster 1994; Priebe and Ferster 2005), as well as in the macaque primary visual cortex (e.g., Carandini et al. 1997). Although no intracellular data in intact animals seem to be available, a slice experiment with the most direct bearing to a linear hypothesis demonstrates this phenomenon in CA1 pyramidal hippocampal cells (Cash and Yuste 1999; Gasparini and Magee 2006).

In line with the second perspective is another optimization issue, which will be affected by linearization of dendritic excitation. Specifically, the energetic cost of computation is of current interest (Attwell and Laughlin 2001; Sarpeshkar 1998; Laughlin and Sejnowski 2003; Levy and Baxter 1996, 2002; Goldberg et al. 2003; Balasubramanian and Berry 2002; Vincent and Baddeley 2003; Vincent et al 2005; Attwell and Gibb 2005). In this regard, quantitative biophysical models are useful to understand the characteristics of evolved computation at the cellular and subcellular levels. The biophysical simulations presented here reveal fundamental interactions between conductances and the metabolic cost of linear dendritic processing.

The simplicity of linearization requires a certain degree of biological complexity, and in this regard the work of Bernander et al. (1994) is seminal. That presentation harnesses voltage-dependent conductances for countering the saturating process of summed synaptic activation. Specifically, voltage-dependent dendritic conductances, including Ca^{2+} and K^{+} channels are used to boost sublinear synaptic summation into linearity. In the time since this work, there have been substantial developments both in terms of knowledge of dendritic ion channels and issues germane to neuronal computation. This increased knowledge is particularly true for the pyramidal neurons of neocortex and hippocampus. These cells focus our attention and motivate us to re-examine the linearization problem, the goal being to fit more recent observations and newer perspectives. Two types of experimental observations are influential.

First, there has been considerable improvement in our parametric knowledge of the A-channel since 1994 (Hoffman et al. 1997; Bekkers 2000). Second, Bernander and colleagues had to guess at the physiological voltages of interest, but today we have a much better idea of the physiological voltage range of forebrain pyramidal neurons under something close to natural conditions. Since most studies indicate that, *in vivo*, a neocortical or hippocampal pyramidal cell will be under constant synaptic bombardment, it will spend most of its time depolarized and much of its time near threshold (from an experimental perspective: Paré et al. 1998, see also Destexhe et al. 2003; Fee 2000; Léger et al. 2005; Steriade et al. 2001; however for exceptions see Crochet and Petersen 2006). Taking such evidence at face value, we attend to neurons under constant synaptic bombardment presumably spending much of their time in a range of −62 to −58 mV with threshold around −55 to −52 mV. These values are significantly hyperpolarized compared to the assumed threshold of the earlier biophysical work and decreases our interest in the voltage-activated calcium conductance considered previously.

A voltage range around −55 mV and experimental observations such as Magee (1999, 2000) focus our main attention on two particular voltage-dependent conductances: persistent sodium (*NaP*) and A-type potassium (*A*) dendritic conductances of these pyramidal cells. Previous work (Morel and Levy 2007) compared the linearization capabilities of the persistent sodium (*NaP*) versus the hyperpolarization-activated mixed cation current (I_h). It was found that there are significant differences between these conductances with the persistent sodium being the better linearizing mechanism over the physiologically relevant voltage-range mentioned above. Here we briefly return to inquiries using I_h and note how it can be used in combination with either I_{NaP} or I_A to enhance the linear range of either current alone.

To summarize, the main goal of this study is to understand the constraints on linearized synaptic responses and to gain some insight into the metabolic cost of linearized excitation. In what follows, we compare the cost of linearization produced with I_{NaP}, I_A, and I_h. The results demonstrate a set of linear relationships between conductance values, cost, and synaptic conductance. At the same time, we show that synaptic gain is constant for any one particular mechanism; likewise the range of linearization is constant. The calculations are constrained by recently reported operating ranges of pyramidal neurons under synaptic bombardment as well as the reported voltage dependence of I_A, I_{NaP}, and I_h. The discussion points out how these calculated metabolic costs can be applied in the constraint-based approach for understanding evolved function.

2 Methods

A biophysically realistic neuron model is properly composed of a soma and many dendritic compartments. Here we focus on a single dendritic compartment containing a variable number of active synapses, a fixed conductance, and one or two voltage controlled conductances. Figure 1

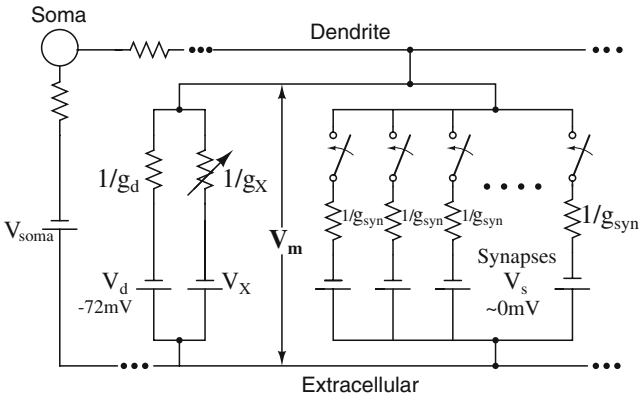

Fig. 1 Equivalent circuit representation of a dendritic compartment under steady-state activation. This analysis is concerned with the dendritic (i.e. non-synaptic) membrane and synaptic parts of the system only. The passive conductance is g_d with V_d its reversal potential; the individual synaptic conductance, g_{syn}, has a reversal potential of V_s; the optional voltage-activated conductance(s) are indicated by g_X and its reversal potential is V_X. The membrane potential is V_m. Somatic elements are shown for reference only and are not considered in this study

presents an equivalent steady-state circuit representation of this compartment.

In this model, we assume that the conductances of the non-synaptic dendritic membrane and the synaptic receptors are close together in the sense that the cytoplastic resistance between them is relatively small and essentially zero compared to other resistances. The resting non-synaptic dendritic conductances are collapsed into g_d, and the active synaptic conductances are collapsed into $g_s = \sum_k g_{syn}$ ($k \in$ active synapses). These only interact through their effects on membrane potential V_m. Finally, it is assumed that synaptic bombardment changes slowly enough compared to neuronal time constants so that, for the time scale of interest, local synaptic and dendritic fluxes are constant, i.e., $dI_s/dt=0$ and $dI_d/dt=0$, respectively.

In order to get a better understanding of the interplay between the different variables, several sets of initial conditions (such as ionic concentrations inside/outside the neuron, total passive non-synaptic dendritic conductance, or quantal synaptic conductance) were studied. We report on the results from one representative set. Table 1 shows the values of variables used in parameterizing the model here, and shows the implied potentials. In this table, T is the temperature; $[x]_{in/out}$ are ion concentrations outside (*out*) or inside (*in*) the cell; and V_i the physiological reversal potentials for the synaptic ($i=s$) and dendritic ($i=d$) parts of the systems. The Nernst equilibrium potentials for the individual ions (E_{Nernst}) are included for reference. Also shown are the permeability ratios for the different conductance pathways at the reversal potential of each conductance.

All synapses are assumed to be AMPA-type excitatory synapses. Each synapse is viewed as being composed of approximately ten channels, each with a channel conductance of 10 pS (in line with published work in pyramidal cells, e.g., Spruston et al. 1995 or Andrasfalvy and Magee 2001), leading to a quantal synaptic conductance of roughly 100 pS (i.e., $g_{syn} \approx 100$ pS). Although a wide range of quantal conductances are reported for forebrain cortical excitatory synapses, the results depend on this choice in only the simplest way (everything scales linearly or is constant, see Table 5). Thus, the selection of $g_{syn}=100$ pS makes it easy to rescale our results without pencil and paper. In the hippocampus, activated NMDA receptors do not make a significant contribution to depolarization and therefore are not included.

The system is analyzed in steady-state, that is, we presume activity levels change more slowly than neuronal time constants (see Hasenstaub et al. 2005 Fig. 2(b), which shows that the power of input fluctuations falls off exponentially after 40 Hz).

As a consequence of steady-state, any change in the total active synaptic conductance (g_s) will directly impact the ionic fluxes of both the non-synaptic dendritic membrane and the synaptic part of the system in producing membrane potential V_m (see Fig. 1). A physiological operating range centered around −60 mV is conjectured, as an approximation of *in vivo* recordings of somatic potentials (e.g., Paré et al. 1998 for data under anesthesia mimicking wakefulness and Fee 2000 for data in awake animals).

The passive dendritic conductance is treated as a fixed parameter but is investigated at several values ranging from $g_d=6.25$ to 50 nS.

Table 1 Representative values of model parameters

Variable	Value	Potential	Value	Conductance	$P_{Na}:P_K$
T	37°C	V_d	−72 mV	Passive dendrite	1:26
$[K^+]_{out}$	4.0 mM	V_s	0 mV	A-type K^+	0:1
$[K^+]_{in}$	140 mM	E^K_{Nernst}	−95 mV	Persistent Na^+	1:0
$[Na^+]_{out}$	145 mM	E^{Na}_{Nernst}	+55 mV	Synaptic	1:0.9
$[Na^+]_{in}$	18.5 mM				

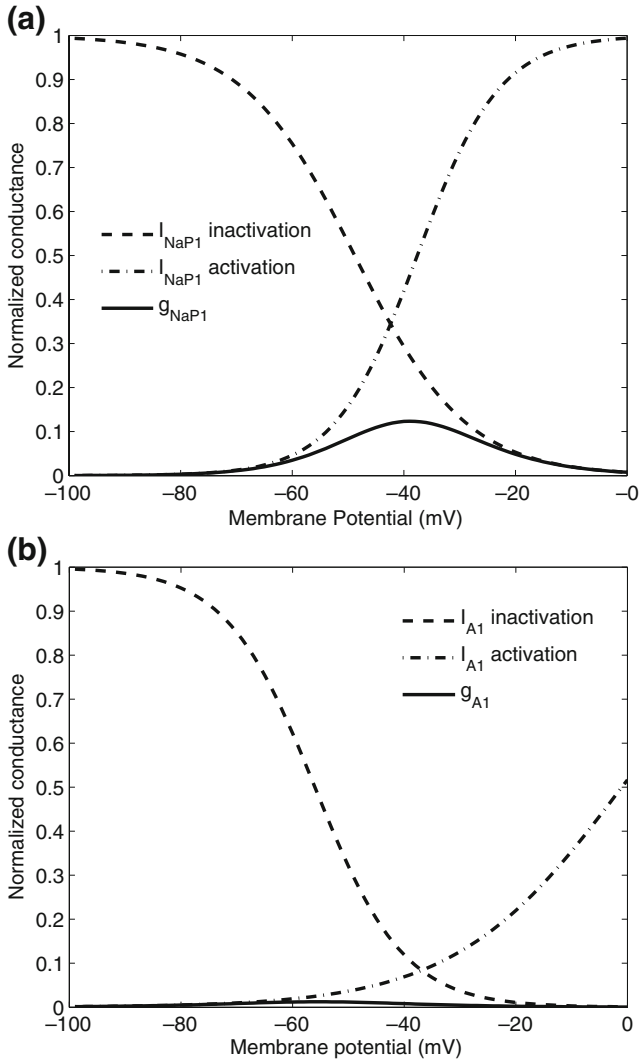

Fig. 2 Typical functional form of voltage-activated conductances. (**a**) The normalized, steady-state, persistent sodium conductance, g_{NaP1}, is adapted from Magistretti and Alonso (1999) for the inactivation data and Agrawal et al. (2001) for the activation data ($\mathrm{I_{NaP1}}$ parameterization). The *dashed line* represents the Boltzmann fit of inactivation data, the *dashed-dotted line* is the equivalent for the activation data, and the *solid line* is the product of the inactivation and activation curves. (**b**) The normalized, steady-state, A-type potassium conductance, g_{A1}, is based on the work of Hoffman et al. (1997) ($\mathrm{I_{A1}}$ parameterization). The *dashed line* represents the Boltzmann fit to inactivation data, the *dashed-dotted line* is the equivalent for activation, and the *solid line* is the product of inactivation and activation curves

2.1 Passive model of a dendritic compartment

As a benchmark, steady-state voltages and currents are evaluated for a passive dendritic compartment under synaptic bombardment. Basic current equations for the dendritic and synaptic parts of the system are $I_d = g_d(V_m(g_s) - V_d)$ and $I_s = g_s(V_m(g_s) - V_s)$, respectively. Each current implicitly includes only sodium and potassium ionic currents whose individual conductances combine to create either g_d or g_s. In steady-state, the sum of the total dendritic and synaptic currents must be zero and therefore $I_s + I_d = 0$ can easily be solved for the steady-state membrane potential $V_m(g_s)$

$$V_m(g_s) = \frac{g_s V_s + g_d V_d}{g_s + g_d} \tag{1}$$

Note that the numerator of Eq. (1) can be further simplified for a synaptic reversal potential of 0 mV.

2.2 Active dendritic conductances as paths to linearization

The passive model is supplemented by active dendritic conductances to produce a linear range of operation. For the subthreshold voltage range of interest, the A-type potassium current (I_A) and the persistent sodium current (I_{NaP}) are the most relevant and constitute a first step. In order to better understand the influence of each channel, they are considered individually and in combination.

Persistent sodium channel A first set of persistent sodium parameters was obtained from the works of Magistretti and Alonso (1999) for the inactivation data and Agrawal et al. (2001) for the activation data, referred to as the $\mathrm{I_{NaP1}}$ parameterization. Their experimentally obtained, voltage-dependent, activation and inactivation curves were fitted with single Boltzmann functions, each with parameter $V_{1/2}$ and associated slope factor (see Fig. 2(a)). At any given voltage, the persistent sodium conductance, g_{NaP1}, is the product of the appropriate points on the steady-state activation and inactivation curves scaled by $\overline{g}_{\mathrm{NaP1}}$, the maximum available channel conductance. This product has the form

$$g_{\mathrm{NaP1}}(V_m) = \overline{g}_{\mathrm{NaP1}} \frac{1}{\left(1 + e^{-(-0.0488 - V_m)/0.010}\right)} \times \frac{1}{\left(1 + e^{(-0.0376 - V_m)/0.0074}\right)} \tag{2}$$

where $\overline{g}_{\mathrm{NaP1}}$ will be adjusted to produce a linear region on the steady-state membrane potential versus total active synaptic conductance curve. Because this channel is known to be homogeneous throughout the neuron, somatic values are used to represent dendritic channels. This set of parameters was previously used in Levy and Morel (2006).

A second set of parameters for the persistent sodium channel was obtained from the work of French et al. (1990) and is labeled $\mathrm{I_{NaP2}}$. Their activation and inactivation parameters were extracted from experimental somatic recordings in neurons from the pyramidal cell layer of the CA1 region and fitted with single Boltzmann functions as

above. The resulting persistent sodium conductance has the same form as Eq. (2) with different parameters. See Appendix B for details of both sets of parameters used.

This channel is assumed to be entirely sodium ion specific (Magistretti and Alonso 1999) and obeying the single ion current equation

$$I_{NaP} = g_{NaP}\left(V_m - E^{\mathrm{Na}}_{\mathrm{Nernst}}\right) \tag{3}$$

where $E^{\mathrm{Na}}_{\mathrm{Nernst}}$ is the Nernst sodium reversal potential, given in Table 1. Note that this parameterization is consistent with that used by Vervaeke et al. (2006) and therefore similar results could be obtained from their choice of values.

A-type potassium channel A first set of activation and inactivation curves obtained from Hoffman et al. (1997), referred as the $\mathrm{I_{A1}}$ parameterization, is used to model this channel. Experimentally obtained activation and inactivation curves (>100 μm from the soma) fitted with single Boltzmann functions in Hoffman et al. (1997) are used to obtain total conductance g_{A1}. This resulted in the solid line of Fig. 2(b), which was then scaled by $\overline{g}_{\mathrm{A1}}$, the maximum available conductance, i.e.,

$$g_{\mathrm{A1}}(V_m) = \overline{g}_{\mathrm{A1}} \frac{1}{\left(1 + e^{-(-0.056 - V_m)/0.008}\right)} \times \frac{1}{\left(1 + e^{(-0.001 - V_m)/0.015}\right)} \tag{4}$$

where $\overline{g}_{\mathrm{A1}}$ will be adjusted to produce a linear region on the steady-state membrane potential vs. total active synaptic conductance curve. Note that very large values of $\overline{g}_{\mathrm{A1}}$ can be expected because of the extremely low probability of channel activation (less than 0.5%) of the available conductance (Fig. 2(b)). This set of parameters was previously used in Levy and Morel (2006).

For comparison, activation and inactivation parameters from Bekkers (2000) were also used to parameterize this potassium channel (>250 μm from the soma). The total conductance has the same form as Eq. (4) with different parameters and this parameterization is labeled $\mathrm{I_{A2}}$. See Appendix B for details of both sets of parameters used.

Unlike the sodium channel, this channel is not assumed to be entirely potassium ion specific although it still obeys the single ion current equation. Equations for this channel are similar to that of the persistent sodium channel, i.e., Eq. (3), after substituting $\mathrm{Na^+}$ for $\mathrm{K^+}$ and g_{NaP} for g_A.

Hyperpolarization activated cation channel The parameters for this non-inactivating, slowly deactivating, mixed cation inward current were obtained from the work of Magee (1998) on dendrites of CA1 pyramidal cells. As with the other channels, the conductance g_h is the product of the steady-state activation curve (Boltzmann fit with voltage of half maximal activation $V_{1/2}$=−90 mV and slope factor k= 8.5 mV) with the maximum available conductance $\overline{g}_h$. See Morel and Levy (2007) for details. The reversal potential for this channel is V_h=+1 mV.

Note that when I_h is included, a dendritic rest potential of V_d=−80 mV is used, compared with −72 mV for the other calculations in this paper. This more hyperpolarized rest potential highlights I_h's contributions, which are stronger at lower membrane potentials.

These dendritic currents were added to the passive system described in the previous section. The sum of the currents therefore becomes

$$I_d(V_m, g_d) + I_s(V_m, g_s) + I_{NaP}(V_m, g_{NaP}) + I_A(V_m, g_A) + I_h(V_m, g_h) = 0. \tag{5}$$

Due to the functional form of the active conductances (e.g., Eqs. (2) and (4)), there is no longer a straightforward analytical solution for the steady-state membrane potential V_m. Numerical simulations are therefore employed.

2.3 Goldman–Hodgkin–Katz formalism for calculation of ion fluxes

Because the Goldman–Hodgkin–Katz (GHK) model of membrane voltage (Goldman 1943; Hodgkin and Katz 1949; Hodgkin and Huxley 1952) is more accurate than the Nernst-potential based calculations in the case of multiple permeating ionic species and a V_m sufficiently far from zero, it is the model of choice for calculating ion fluxes.

As noted before, only $\mathrm{Na^+}$ and $\mathrm{K^+}$ ions are explicitly included in each part (dendritic membrane and synapses) of the dendritic compartment. Therefore, the GHK ionic current equations (similar to those of Hodgkin and Katz 1949, Eqs. (2·3) and (2·4)) are

$$I_{Na} = P_{Na} \frac{F^2 V_m}{RT} \frac{[\mathrm{Na^+}]_{\mathrm{in}} - [\mathrm{Na^+}]_{\mathrm{out}} e^{\left(\frac{-V_m F}{RT}\right)}}{1 - e^{\left(\frac{-V_m F}{RT}\right)}} \tag{6}$$

$$I_K = P_K \frac{F^2 V_m}{RT} \frac{[\mathrm{K^+}]_{\mathrm{in}} - [\mathrm{K^+}]_{\mathrm{out}} e^{\left(\frac{-V_m F}{RT}\right)}}{1 - e^{\left(\frac{-V_m F}{RT}\right)}} \tag{7}$$

Here $[x]_{\mathrm{in}}$, $[x]_{\mathrm{out}}$ are ion concentrations inside and outside the cell respectively; F is Faraday's constant; R is the gas constant; T is the temperature; and P_x the ionic permeability of species x. For the system under study, it is assumed that the ratio of permeabilities P_{Na}/P_K is different for the dendritic membrane and the synapses. Consequently, there exists one reversal (GHK) potential for the

dendritic membrane part of the system, V_d, and another for the synapses, V_s (see Table 1).

The value of P_K, or even the ratio P_{Na}/P_K, is not directly available for the conductances used here (and most any other conductance). As is typical (e.g., Hodgkin and Huxley 1952), we use the GHK equation conductance and reversal potential measurement to infer the necessary permeabilities. We convert the usual (Hodgkin and Katz 1949) development to chord conductance and go one step further by assuming our system is at a steady-state and not necessarily at its reversal potential. That is, average synaptic bombardment is maintained long enough to charge the membrane capacitance in our simplified dendritic compartment.

The chord conductances, $g_i = I_i/(V_m - V_i)$ where $I_d = I_{K_d} + I_{Na_d}$ for the dendrite and $I_s = I_{K_s} + I_{Na_s}$ for the synapses, are therefore inverted and solved for permeabilities P_{K_i} such that

$$P_{K_i} = \frac{RTg_i}{F^2 V_m} \times \frac{(V_m - V_i)\left(1 - e^{\frac{-V_m F}{RT}}\right)}{[\mathrm{K}^+]_{\mathrm{in}} - [\mathrm{K}^+]_{\mathrm{out}} e^{\frac{-V_m F}{RT}} + \left[\frac{P_{Na}}{P_K}\right]_i \left([\mathrm{Na}^+]_{\mathrm{in}} - [\mathrm{Na}^+]_{\mathrm{out}} e^{\left(\frac{-V_m F}{RT}\right)}\right)} \tag{8}$$

where $\left[\frac{P_{Na}}{P_K}\right]_i$ and V_i are, respectively, the ratio of permeabilities and reversal potential of system i ($i \in$ {dendrite, synapse}). For the synaptic subsystem, g_i is replaced by g_s, a function of the number of active synapses, while g_i is assigned the value of g_d for the non-synaptic dendritic membrane. After each substitution, the appropriate form of P_{K_i} obtained from Eq. (8) can be inserted into the current Eqs. (6) and (7), with P_{NaP_i} related to P_{K_i} via ratios $[P_{Na}/P_K]_i$. The results report the total potassium current versus total active synaptic conductance where the total potassium current uses separately Eq. (7) for the dendrite and the synapses.

The steady-state calculations yield a simple mapping between synaptic conductance and membrane potential when solving Eq. (1). When one or more voltage-activated conductances are involved, the appropriate version of Eq. (5) is then solved numerically using *MATLAB*. Sweeps over values of $\overline{g}_A$ and/or $\overline{g}_{NaP}$ were performed to discover the greatest voltage range (as determined initially by visual inspection) of linear synaptic response. This maximal range (as a function of total synaptic conductance) is then characterized by the average single-synapse depolarization within this range. Arbitrarily, we define the limits of each range as a variation of single synapse depolarization of ±2% around the average value. Using the computed solutions for each equation, the different ranges of linearizable synaptic conductances can in turn be translated into corresponding ranges of steady-state membrane potential.

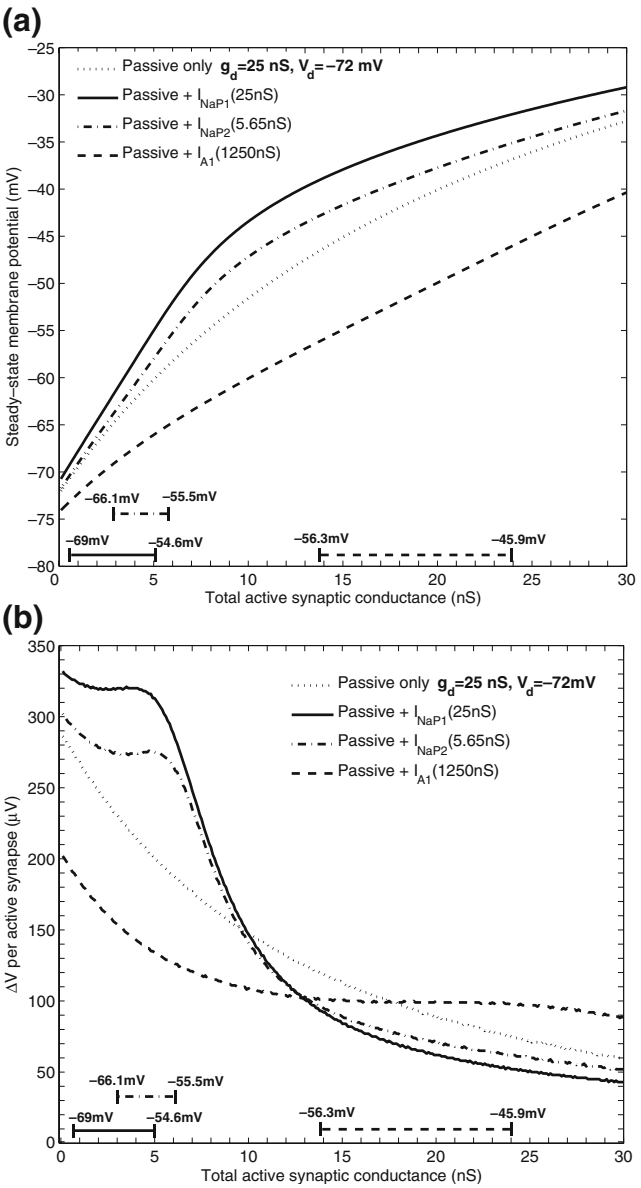

Fig. 3 Linearizing effect of three voltage-activated conductances for g_d=25 nS (V_d=−72 mV). (**a**) Voltage of the systems as a function of steady-state activation. The *dotted line* represents a system with a passive dendrite only, the *dashed line* indicates the passive system with the addition of an A-type K^+ current (I_{A1} parameterization), the *solid line* shows the passive system plus a persistent Na^+ dendritic channel (I_{NaP1} parameterization), and the *dashed-dotted line* represents the passive system with a persistent Na^+ channel (I_{NaP2} parameterization). It can be seen that I_{NaP}'s main effect is to further depolarize the system compared to the passive only level. In contrast, I_A hyperpolarizes the system compared to the passive level. Values of $\overline{g}_A$ and $\overline{g}_{NaP}$ are given in parentheses for each curve in the legend. Interval markers at the bottom of each graph indicate the ranges of linearization: *solid line* for I_{NaP1}-enhanced system, dashed-dotted for I_{NaP2}-enhanced system, and *dashed line* for a system with I_{A1}. (**b**) Contribution to the depolarization of the steady-state membrane potential by each additional active synapse. Note that the regions of constant contribution are the linearized ones and are indicated by *horizontal lines above the abscissa*: i.e., 0.5–5 nS for the system with I_{NaP1}, 2.8–5.8 nS for the system with I_{NaP2}, and 13.7–23.9 nS when I_{A1} is present. Legend is the same as for graph (**a**)

2.4 Energy cost of ionic currents

In the course of steady-state synaptic bombardment, the cost of dendritic computation arises from the cost of maintaining the ion gradients. Such maintenance depends on the Na^+/K^+ ATPase pump.

One cycle of this ionic pump consumes one ATP molecule and pumps out three sodium ions while two potassium ions are brought in. In the steady-state, Na^+ and K^+ fluxes are equal. This imbalance between fluxes and pump is problematic in terms of specification of its resolution. However, its generic resolution is straight forward for sodium ions as they are used to power a variety of other pumps. Additional, constantly present, metabolic fluxes may explain the third Na^+. Such sodium dependent metabolic transport includes HCO_3^-, glucose, glutamate, and Ca^{2+}. Thus, it is our position that either Na^+ or K^+ steady-state fluxes are suitable for measuring the metabolic energy needs.

We understand that not everyone agrees with the fate of the third Na^+ that is pumped per ATP (e.g., Attwell and Laughlin 2001). Fortunately, alternative formulations do not change the fundamental relationships here. That is, one can rescale the energy consumed by a constant consistent with one's personal theory of the fate of the third Na^+.

3 Results

3.1 General aspects of linearization

In the absence of voltage-dependent conductances, increasing levels of synaptically produced depolarization lead to a progressively weaker contribution by each additional, active synapse. However, judiciously including either I_A or I_{NaP}, or a combination of both, linearizes this sublinear effect; unfortunately this linear range is limited.

Figure 3(a) illustrates the progressive depolarization of the steady-state membrane potential as the number of active synapses increases for four models: the passive dendrite model (dotted line), the passive model enhanced by two different parameterizations of I_{NaP} (see Section 2, the solid line for I_{NaP1}, the dashed-dotted line for I_{NaP2}), and the passive model enhanced by I_{A1} (dashed line). As a function of total active synaptic conductance, the I_{NaP}-enhanced models ride above the passive model while the I_{A1}-enhanced model sits below the passive-model. The linearizing amplifications for I_{NaP} occur, roughly, between −69 mV and −55 mV (I_{NaP1} model) or −66 mV and

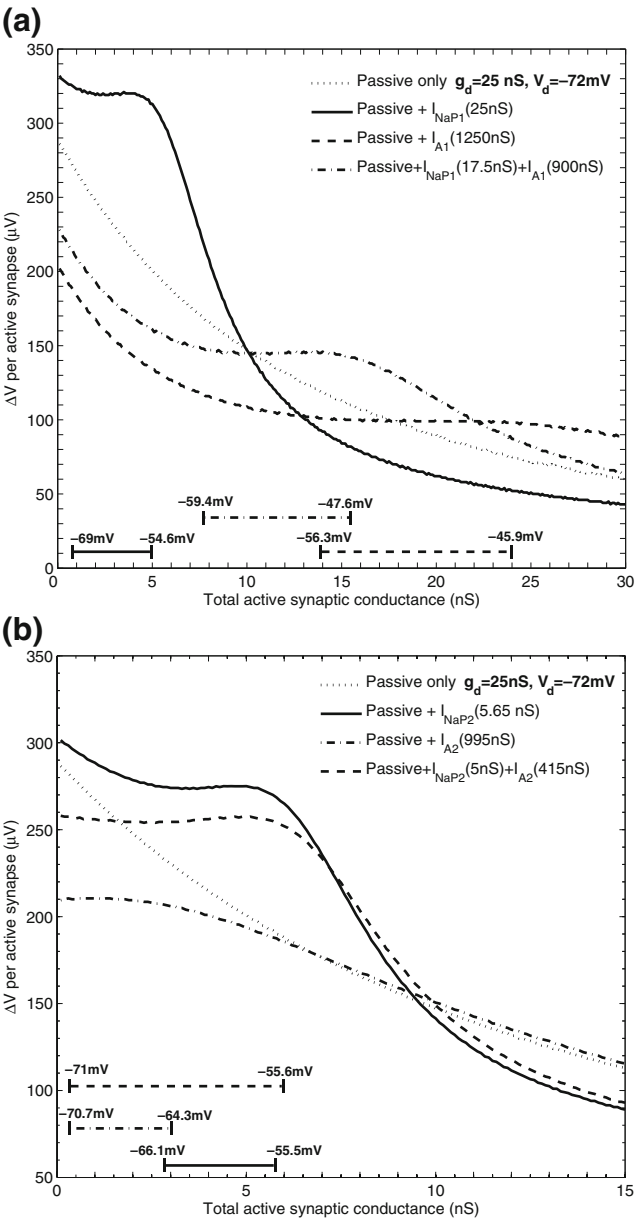

Fig. 4 Judiciously combining *NaP*- and *A*-conductances produces intermediate ranges of linearization which are wider than the range for *NaP* alone. (**a**) The linear range produced by this blend (passive plus I_{NaP1} and I_{A1}) of conductances is slightly longer than that of the system with persistent sodium only (8 nS in length as indicated by the *dashed-dotted interval marker*) although not longer than the A-type potassium-only results. Depolarization per additional active synapse for the passive only system (g_d=25 nS, V_d=−72 mV) is shown by the *dotted line*. The passive plus I_{NaP1} only ($\overline{g}_{NaP1} = 25$ nS) is the *solid line* and the I_{A1}-enhanced system ($\overline{g}_{A1} = 1250$ nS) is represented by the *dashed line*. The *dashed-dotted line* represents a system where both active conductances have been added ($\overline{g}_{NaP1} = 17.5$ nS and $\overline{g}_{A1} = 900$ nS). Linear ranges are indicated by their respective *interval makers at the bottom of the graph*. (**b**) Another example of active conductances (I_{NaP2} and I_{A2}) combined to form a different linear range. Again the combined linear range is located between the linear ranges produced by using individual conductances. The length of the range is also longer, in terms of total active synaptic conductance, 0–6.1 nS, and steady-state membrane potential, 15.4 mV (as indicated by the *dashed interval marker*), than the ranges produced by individual conductances. See Section 2 and Fig. 2 for voltage dependencies

−55 mV (I_{NaP2} model) while the linearization produced by I_{A1} lies between −56 mV and −45 mV.

These linear ranges are easier to see in Fig. 3(b). This figure shows the depolarization caused by adding one more active synapse (100 pS) as a function of the number of active synapses. As shown in Fig. 3(b), the g_A conductance, compared to g_{NaP}, is better suited for linearizing under heavy synaptic bombardment. However, under such heavy bombardment, the depolarization per 100 pS synapse is necessarily lower. The models with the persistent sodium channel are linear for ranges between 0.5 and 5.8 nS of total synaptic conductance. In this range, a single synaptic event is 320 μV (I_{NaP1} model) or 274 μV (I_{NaP2} model). A much higher, linearized conductance range characterizes the I_{A1}-enhanced model. Specifically, that range is 13.7 to 24 nS. The wider range using g_A is accompanied by smaller synaptic events (100 μV).

Figure 3(b) also shows, by comparison with the simple passive model, that I_{NaP} is amplifying single synaptic events. In contrast, I_A works by de-attenuating. The net result, compared to the passive model, is smaller synaptic responses at lower excitation and larger synaptic responses at higher excitation.

By combining I_{NaP} and I_A many different linearizing ranges can be produced. Figure 4(a) illustrates one such combination where ($I_{NaP1}(\overline{g}_{NaP1} = 17.5\ \text{nS})$) and ($I_{A1}(\overline{g}_{A1} = 900\ \text{nS})$) are combined with the passive system. For this combination, the linearized voltage range is −59 to −47 mV. In this range, the depolarization by one, 100 pS synapse is 145 μV. In this case, compared to I_{NaP1} alone, the linear range handles almost twice the total synaptic conductance and is shifted down and to the right under the influence of the additional potassium conductance. Other combinations of $\overline{g}_{NaP1}$ and $\overline{g}_{A1}$ shift the position of the linearized range. Figure 4(b) illustrates the combination of ($I_{NaP2}(\overline{g}_{NaP2} = 5\ \text{nS})$) and $I_{A2}(\overline{g}_{A2} = 415\ \text{nS})$. In this instance, the linearized voltage range is −71 to −55 mV, and in this range, the depolarization by one, 100 pS synapse is 256 μV.

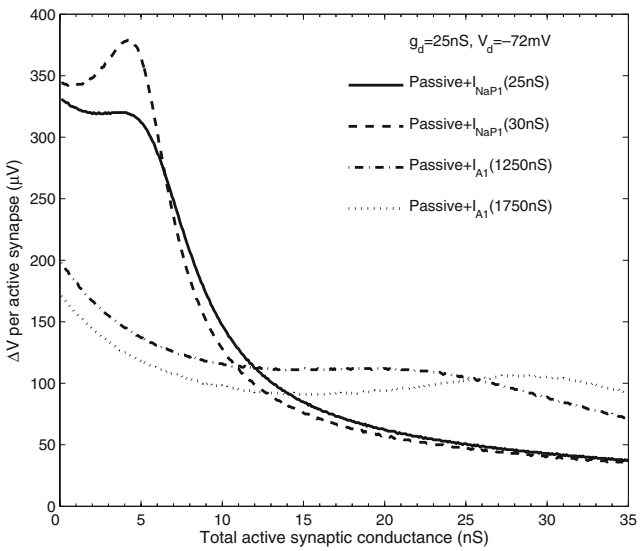

Fig. 5 Linearity gives way to supralinearity when too much I_{NaP} (or I_A) is added to the passive system (g_d=25 nS). The addition of I_{NaP1} ($\overline{g}_{NaP1} = 25$ nS) to the passive system produces a linearized range of 4.5 nS (0–5 nS of total active synaptic conductance) but this range is reduced to 2 nS when $\overline{g}_{NaP1}$ is increased to 30 nS. Similarly, the addition of $I_{A1}(\overline{g}_{A1} = 1,250\ \text{nS})$ creates a linearized range of 10.2 nS in length but is reduced to 7.1 nS when $\overline{g}_{A1}$ is increased to 1,750 nS

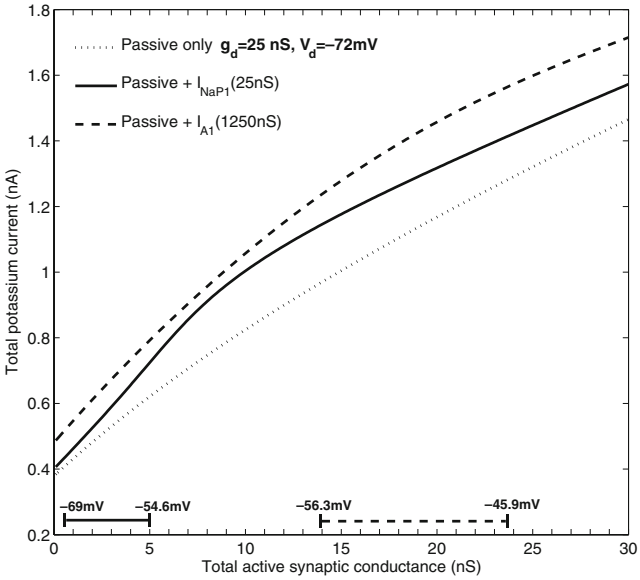

Fig. 6 Metabolic cost as a function of the total active synaptic conductance for g_d=25 nS (V_d=−72 mV). The total K^+ current increases with the addition of either active dendritic conductance although the persistent Na^+ is seen to be relatively less costly (over its linear range) than the A-type potassium channel. The legend indicates which parameterizations are used and the *horizontal interval markers* indicate each relevant linear range (the *solid line* indicates the passive + I_{NaP1} system and the *dashed* line indicates the passive + I_{A1} system)

After examining the metabolic costs, more details will be provided relating conductance values to several of the parameters.

3.2 Linearizing ranges are constrained

The linearized ranges cannot be arbitrarily extended. There are unavoidable interactions between baseline conductance g_d, and maximum useful channel conductances $\overline{g}_{NaP}$ and $\overline{g}_A$; these interactions constrain the linearizing ranges. Obviously, too little $\overline{g}_{NaP}$ (or too little $\overline{g}_A$) will leave the original regime sublinear; on the other hand, too much $\overline{g}_{NaP}$ (or too much $\overline{g}_A$) defeats linearity by producing supralinear effects. Thus the ranges of linearization are limited, and such limitations are solely related to the value of g_d when the voltage dependencies and driving batteries are constant. Figure 5 compares linear and supralinear examples by plotting the voltage of an additional, single synaptic event as a function

Table 2 Characteristics of linear regions obtained from systems incorporating persistent sodium conductances for selected values of g_d

g_d (input resistance at rest)	6.25nS (160MΩ)	12.5nS (80MΩ)	25nS (40MΩ)	50nS (20MΩ)
Passive ΔV per 100 pS synapse (for first active synapse)	1132 μV	570 μV	286 μV	142 μV
I_{NaP1} model				
$\overline{g}_{NaP1}$ (to linearize)	6.25 nS	12.5 nS	25 nS	50 nS
Linear range characteristics:				
Voltage	−61.8±7.2 mV	−61.8±7.2 mV	−61.8±7.2 mV	−61.8±7.2 mV
Synaptic gain	1.37±0.18	1.37±0.18	1.37±0.18	1.37±0.18
Total synaptic conductance	0.65±0.55 nS	1.3±1.1 nS	2.75±2.25 nS	5.5±4.5 nS
# active synapses (100 pS/syn)	6.8±5	13.7±11.2	27.5±22.5	55±45
ΔV per 100 pS synapse	1280±25 μV	640±12 μV	320±6 μV	160±3 μV
Cost (total I_{K^+})	0.16±0.05 nA	0.32±0.09 nA	0.65±0.19 nA	1.30±0.39 nA
I_{NaP2} model				
$\overline{g}_{NaP2}$ (to linearize)	1.41 nS	2.82 nS	5.65 nS	11.3 nS
Linear range characteristics:				
Voltage	−60.8±5.3 mV	−60.8±5.3 mV	−60.8±5.3 mV	−60.8±5.3 mV
Synaptic gain	1.27±0.15	1.27±0.15	1.27±0.15	1.27±0.15
Total synaptic conductance	1.07±0.37 nS	2.15±0.75 nS	4.3±1.5 nS	8.6±3 nS
# active synapses (100 pS/syn)	10.7±3.7	21.5±7.5	43±15	86±30
ΔV per 100 pS synapse	1096±22 μV	548±11 μV	274±5.5 μV	137±2.7 μV
Cost (total I_{K^+})	0.17±0.03 nA	0.35±0.07 nA	0.70±0.15 nA	1.40±0.30 nA

of total active synaptic conductance. A passive dendritic conductance of 25 nS combined with $\overline{g}_{NaP1} = 25$ nS produces a linear range of 4.5 nS (0.5 to 5 nS). However, increasing the value of $\overline{g}_{NaP1}$ to 30 nS decreases the linear range to 2 nS. In the I_{A1}-augmented system, a $\overline{g}_{A1}$ value of 1,250 nS produces a linearized range of 10.2 nS (13.7 to 23.9 nS of total active synaptic conductance). However, increasing the value of $\overline{g}_{A1}$ to 1,750 nS decreases the length of the range to 7.1 nS. Linearizing combinations of I_A and I_{NaP} are similarly restricted (data not shown).

3.3 Metabolic cost

Linearizing synaptic excitation has its metabolic costs. The graph of Fig. 6 illustrates the costs of adding either I_A or I_{NaP} where cost is quantified as total potassium current (sum of dendritic and synaptic currents, see Section 2).

In the case of the I_{NaP1}-enhanced model, the additional cost seems quite modest. For example, at the extreme upper end of the linear range (g_s=5 nS), the metabolic cost is 11.4% higher (0.85 nA with I_{NaP1} versus 0.76 nA for passive only); at the other end of the range (g_s=0.5 nS), the presence of I_{NaP} increases cost by 6.2% (0.45 nA with I_{NaP1} versus 0.43 nA for passive only).

In the case of adding only I_A to the passive system, clear intuition is difficult because decreasing conductance leads to less flux but the baseline polarization of the linear range is more costly. Calculations resolve the confusion. Due to the high baseline fluxes, the I_{A1}-augmented system is consistently more expensive when compared to the passive system. Even at the upper end of its linear range (g_s=24 nS), with its rate of cost-increase still decreasing, the large baseline current makes this system 29% more costly that the passive system (1.97 nA with I_{A1} versus 1.52 nA for passive only, see Fig. 6). Unfortunately, the costly baseline conductance seems inevitable since its presence is necessary if the I_{A1}-enhanced model is to turn off an appropriate amount of conductance. Tables 2 and 3 present results for selected values of g_d to facilitate comparisons between systems.

Although it would appear that I_A augmented systems are consistently more costly, there are other ways to compare any two systems. For example, when producing the same amount of depolarization-per-additional-active-synapse, the difference in the total potassium current does not always favor the same system as described above. That is, the model enhanced by I_{NaP1} costs 0.51±0.12 nA when the linear range is set to produce 400 μV synaptic depolarizations (which requires g_d=21.8 nS with 24 active synapses,

Table 3 Characteristics of linear regions obtained from systems incorporating A-type potassium conductances for selected values of g_d

g_d (input resistance at rest)	6.25nS (160MΩ)	12.5nS (80MΩ)	25nS (40MΩ)	50nS (20MΩ)
Passive ΔV per 100 pS synapse (for first active synapse)	1132 μV	570 μV	286 μV	142 μV
	I_{A1} model			
$\overline{g}_{A1}$ (to linearize)	312.5 nS	625 nS	1250 nS	2500 nS
Linear range characteristics:				
Voltage	−51.1±5.2 mV	−51.1±5.2 mV	−51.1±5.2 mV	−51.1±5.2 mV
Synaptic gain	1.07±0.24	1.07±0.24	1.07±0.24	1.07±0.24
Total synaptic conductance	4.7±1.2 nS	9.4±2.5 nS	18.8±5.1 nS	37.7±10 nS
# active synapses (100 pS/syn)	47±12	94±25	188±51	377±100
ΔV per 100 pS synapse	400±8 μV	200±4 μV	100±2 μV	50±1 μV
Cost (total I_{K^+})	0.44±0.05 nA	0.88±0.10 nA	1.76±0.21 nA	3.5±0.42 nA
	I_{A2} model			
$\overline{g}_{A2}$ (to linearize)	247.5 nS	495 nS	995 nS	1980 nS
Linear range characteristics:				
Voltage	−67.5±3.2 mV	−67.5±3.2 mV	−67.5±3.2 mV	−67.5±3.2 mV
Synaptic gain (attenuation)	0.81±0.08	0.81±0.08	0.81±0.08	0.81±0.08
Total synaptic conductance	0.3±0.3 nS	0.7±0.7 nS	1.5±1.5 nS	3.1±3.1 nS
# active synapses (100 pS/syn)	3.8±3.8	7.7±7.7	15.5±15.5	31±31
ΔV per 100 pS synapse	840±16 μV	420±8.4 μV	210±4.2 μV	105±2.1 μV
Cost (total I_{K^+})	0.14±0.02 nA	0.29±0.04 nA	0.59±0.09 nA	1.19±0.19 nA

not shown). In contrast, for the I_{A1}-enhanced model that also produces 400 μV depolarizations (at g_d=6.25 nS with 47 active synapses), the costs are 0.44±0.05 nA over its linear region. This represents a 15% (mid-range) increase from the I_{A1} to the I_{NaP1} system, with the I_{A1}-enhanced system clearly ahead.

Yet another interesting comparison is one in which the number of active synapses is the same across systems but g_d is different for the two systems. For example, if we compare costs for two of the augmented systems when 55 synapses are active in the center of each linear range, the I_{A1}-enhanced system is again the least expensive (0.51 nA

Table 4 Characteristics of linear regions obtained from systems incorporating both persistent sodium and A-type potassium conductances for selected values of g_d

I_{Nap} I_A	I_{NaP1} I_{A1}	I_{NaP2} I_{A1}	I_{NaP1} I_{A2}	I_{NaP2} I_{A2}
g_d	25 nS	25 nS	25 nS	25 nS
$\overline{g}_{NaP}$ and $\overline{g}_A$ (to linearize)	17.5 and 900 nS	5 and 900 nS	15 and 580 nS	5 and 415 nS
Linear range characteristics:				
Voltage	−53.5±5.9 mV	−56.8±3.9 mV	−65.3±5.2 mV	−63.3±7.7 mV
Synaptic gain	1.08±0.21	0.99±0.13	1.03±0.13	1.12±0.21
Total synaptic conductance	11.7±4 nS	10.1±2.6 nS	2±2 nS	3±3 nS
# active synapses (100 pS/syn)	117±40	101±26	20±20	30±30
ΔV per 100 pS synapse	145±2.9 μV	145±2.9 μV	256±5.1 μV	256±5.1 μV
Cost (total I_{K^+})	1.36±0.23 nA	1.28±0.18 nA	0.61±0.14 nA	0.65±0.22 nA

Table 5 Linear relationships between some of the variables in the model

Conductance:	*NaP*		*A*	
Parameterization:	I_{NaP1}	I_{NaP2}	I_{A1}	I_{A2}
$\overline{g}_X/g_d$ to linearize	1	0.22	50	39.6
# of active synapses in center of linear range	$0.11 \times \frac{g_d}{g_{syn}}$	$0.17 \times \frac{g_d}{g_{syn}}$	$0.75 \times \frac{g_d}{g_{syn}}$	$0.06 \times \frac{g_d}{g_{syn}}$
ΔV_{syn} in linear range	$\frac{g_{syn}}{g_d} \times 80$ mV	$\frac{g_{syn}}{g_d} \times 68.5$ mV	$\frac{g_{syn}}{g_d} \times 25$ mV	$\frac{g_{syn}}{g_d} \times 52.5$ mV
Cost in center of linear range (K^+ current)	$g_d \times 26$ mV	$g_d \times 28$ mV	$g_d \times 70$ mV	$g_d \times 23$ mV

with I_{A1} at g_d=7.3 nS versus the 1.16 nA with I_{NaP1} with g_d=50 nS). Thus if g_d is quite small, the I_A model is much more efficient than the I_{NaP} system. This suggests an I_A advantage at more distal locations.

3.4 Generalizing the results

This section and the accompanying tables will help the reader who wants to apply linearizations at different rest conductances (for example, the conductance to ground will vary across the dendritic axis). In sequence, Tables 2, 3, and 4 present the interactions with g_d for *NaP*, *A*, and four combinations of *NaP* and *A*. Finally, Table 5 abstracts the constants of the linear dependencies covered in the preceding three tables.

Once the voltage-dependent conductances are specified, the two parameters unaffected by variations of g_d are: a) the linearized voltage range and b) the synaptic gain (defined as $\Delta V_{active}/\Delta V_{passive}$). For the I_{NaP}-enhanced system, the voltage range of linear synaptic activity is −61.8±7.2 mV (I_{NaP1} parameterization**)** while for the system containing $I_{A1,}$ it is −51.1±5.2 mV. The relationship also holds when more than one voltage-activated conductance is present (data not shown). Equally noteworthy is the fact that the synaptic gain remains constant across varying values of g_d. Taking I_{NaP1} as an example, there is a constant synaptic gain of 1.37±0.18 across the linear range while for I_{A1} the constant synaptic gain is 1.07±0.24.

As opposed to the two parameters that do not change with g_d, in each linearized range four parameters are linearly related to g_d: **(**1**)** the total synaptic conductance in the linear range; or equivalently, (2**)** the number of active synapses of fixed conductance in the linear range; (3**)** the depolarization produced by one more active synapse; and (4**)** the metabolic cost of one more active synapse.

Tables 2 and 3 document that, as the value of g_d increases, the total synaptic conductance characterizing the linear region proportionally increases. For example, in the case of the system incorporating I_{NaP1}, the conductance range changes from 0.65±0.55 nS at g_d=6.25 nS to 5.5± 4.5 nS at g_d=50 nS. It can be noted that an 8-fold increase in g_d leads to a linear region that is 8 times longer (~1.1 ns to 9.0 ns). Similarly, in the I_{A1}-augmented system, the conductance of the linearized range changes from 4.7± 1.2 nS (g_d=6.25 nS) to 37.7±10 nS (g_d=50 nS). Again the linear relationship between the value of g_d and the length of the linear region is apparent (~2.4 to 20 nS).

While the number of 100 pS active synapses in the linear region is proportional to g_d, the depolarization produced by a single synaptic event over the same range must, for consistency, be inversely proportional to the value of g_d (see Appendix A for additional details). Indeed, in the I_{NaP1}-enhanced system, the ΔV per additional synapse is 1,280± 25 μV at g_d=6.25 nS with 6.8±5 active 100 pS-synapses versus 160±3 μV (55±45 active synapses) when g_d=50 nS. These linear relationships can be generalized in Table 5.

Although not shown, similar relationships can be derived in models using more than one conductance (e.g., using the different values given in Table 4).

Table 5 summarizes linear relationships relative to g_d and synaptic conductance g_{syn}. The first row of Table 5 reports the scaling constants that produce linearization for the various conductances as a function of g_d. For example, $\overline{g}_{NaP1}/g_d$ is one and $\overline{g}_{A1}/g_d$ is fifty. The second row shows the number of active synapses at the center of the linear range as a function of g_d and $g_{syn.}$ For example, with I_{NaP1} alone, the number of active synapses in midrange is $0.11 \times \left(g_d/g_{syn}\right)$. Likewise, at the center of the linear range, as seen in row three, ΔV per additional synapse is equal to $\left(g_{syn}/g_d\right) \times 80$ mV.

Due to the direct relationship between g_d and $\overline{g}_{NaP}$ or $\overline{g}_A$ (row one), varying g_d also affects the metabolic cost. Specifically, since g_d also fixes the total synaptic conductance in midrange, increasing g_d causes proportionate increases in current. For example, for I_{NaP1} the cost at the center of the linear range is $g_d \times 26$ mV while for the I_A enhanced model (I_{A1}), that cost is $g_d \times 70$ mV.

3.5 Comparison with the hyperpolarization activated current

Previously, we examined the contributions of I_{NaP} and I_h (Morel and Levy 2007). At the perspicacious suggestion of a reviewer, we reconsider models with I_h.

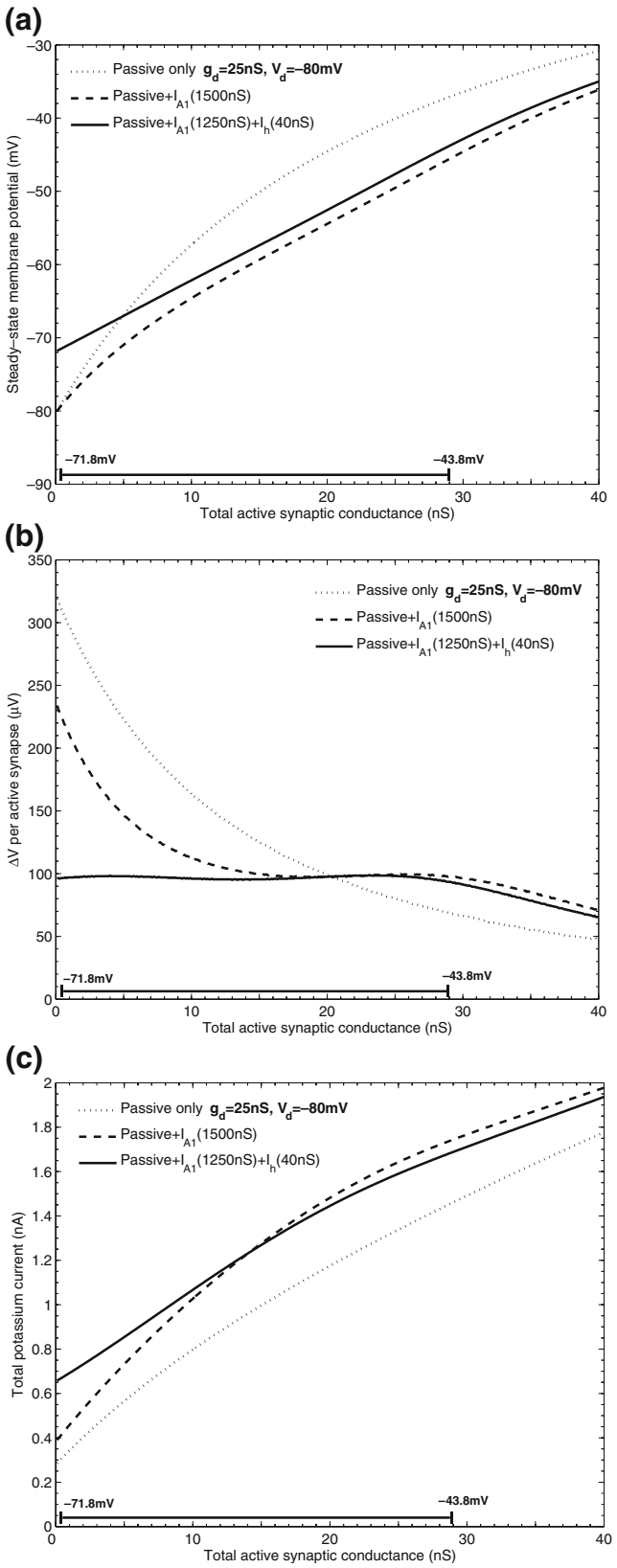

Fig. 7 Combining I_h with I_{A1} produces the longest linear range. (**a**) Voltage of the systems as a function of steady-state activation. The *dotted line* represents a system with a passive dendrite only (g_d= 25 nS, V_d=−80 mV), the *dashed line* indicates the passive system with the addition of an A-type K^+ current (I_{A1} parameterization), and the *solid line* represents a system where two active conductances have been added ($\overline{g}_{A1}$ = 1250 nS and $\overline{g}_h$ = 40 nS). (**b**) Contribution to the depolarization of the steady-state membrane potential by each additional active synapse. (**c**) The effect of I_h on I_{A1}-alone costs are mixed. Addition of I_h to I_{A1} results in lower costs under heavy bombardment (ca. −57 to −44 mV), but at the lowest level of excitation, adding I_h almost doubles the rest cost. Parameterization for I_h is from Magee (1998), see Section 2 for details

The g_A and g_h conductances can be combined to produce, what is here, the greatest observed linear range. As can be seen in Fig. 7, this combination (40 nS of $\overline{g}_h$ and 1,250 nS of $\overline{g}_{A1}$) implies a linearized range from the rest value of −71.8 mV (0 active synapses) all the way to a depolarization value of −43.8 mV. This latter value corresponds to 290 active synapses. One penalty for such a long range is a small synaptic event. Assuming a synaptic event of 100 pS, each synapse contributes only 96 μV of depolarization at the dendrite (Fig. 7(b)), and presumably less at the soma. Of course, increasing the individual synaptic event conductance will proportionally increase the individual depolarization while increasing the number of active synapses in the linear range.

This mixed cation conductance, I_h, can be used in combination with I_{NaP} to extend the linearization range of I_{NaP2} alone in much the same manner that I_A can be combined with an I_{NaP} (Fig. 8). Indeed, from the perspective of the length of the linear range, I_h and I_{A2} seem equally good (20.5 mV vs. 19.2 mV) when combined with I_{NaP2} (whose linear range alone is 10.6 mV; see Fig. 8(b) and Table 4 for details). However, the costs of these linearizations provide further ground for choosing a particular combination. As shown in Fig. 8(c), I_h combined with I_{NaP2} is less expensive than I_{A2} plus I_{NaP2}. Therefore, given their similar voltage ranges, the I_h combination should be preferred.

A similar comparison between the I_h plus I_{A1} model versus the I_h plus I_{NaP2} model is problematic because the desirable longer range accompanies an undesirable increase of metabolic costs. Comparing across Figs. 7(c) and 8(c), the 28 mV linearized voltage range of Fig. 7(c) is much more costly. This longer range of I_h plus I_{A1} costs 80% more at zero active synapses, and when both systems are depolarized to −55.8 mV, the I_h plus I_{A1} costs 60% more than the I_h plus I_{NaP2} system.

4 Discussions

The non-synaptic dendritic membrane of neurons contains many voltage-activated conductances, although their role in

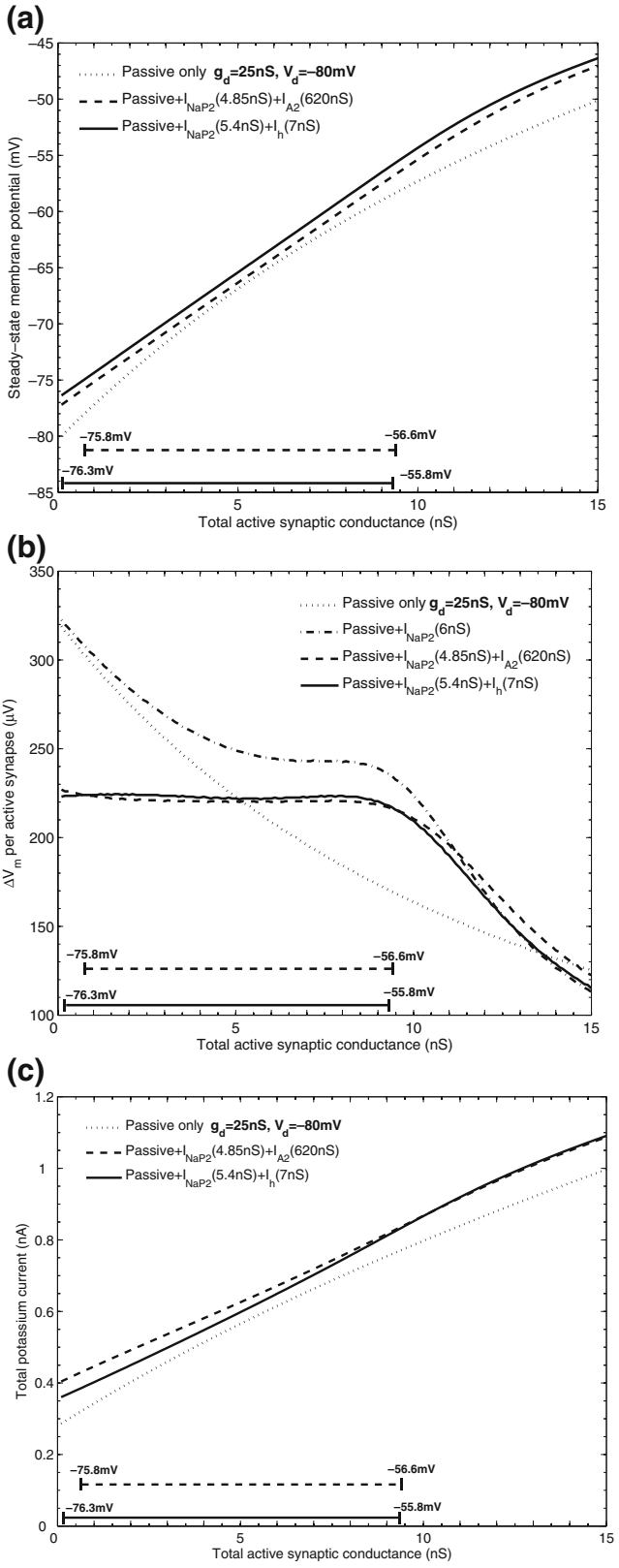

Fig. 8 The combination of the g_h and g_{NaP2} conductances is less costly than g_{A2} plus g_{NaP2} for similar linear ranges. (**a**) Voltage of the systems as a function of steady-state activation. The *dotted line* represents a system with a passive dendrite only (g_d=25 nS, V_d= −80 mV), the *solid line* shows the passive system plus I_{NaP2} and I_{A2}, and the *dashed line* represents the passive system with I_{NaP2} and I_h. (**b**) The addition of either I_h or I_{A2} extends I_{NaP2}'s linear range by more than 10 mV. The *dashed-dotted line* indicates the passive system with the addition of the persistent Na^+ current (I_{NaP2} parameterization). (**c**) Although the extended ranges are comparable, the combination with I_h is less costly. Note that in graphs (**a**) and (**b**) the Passive plus I_{NaP2} line has been omitted for clarity. Parameterization for I_h is from Magee (1998), see Section 2 for details

synaptic integration is still subject to much discussion (see, for example, Johnston et al. 1996; Yuste and Tank 1996; Magee et al. 1998; Magee 2000; Gulledge et al. 2005 for reviews). The various positions taken in theses articles are not necessarily incompatible. For example the simple, single compartment, steady-state linearization model considered here is consistent with other interpretations. In Magee and Cook (2000), there is the report of increasing synaptic conductance as distance from the cell body increases. They also observe that $\overline{g}_A$ grows from proximal to distal loci. Their interpretation of equalizing synaptic events occurring up and down the dendritic axis is consistent with our linearizing perspective. Moreover, their observation of increasing $\overline{g}_A$ with distance from the soma is predicted by the linearization perspective, particularly when synaptic depolarization is larger at more distal locations. In order for linearization to extend up the dendrite, and if there is to be stronger synapses distally, the range of linearization must extend in the depolarizing direction. This requirement fits well with observations (see Hoffman et al. 1997 or Bekkers 2000) that I_A channel density increases with distance from the soma and the observations here. Similarly, the observations here make sense of the higher concentrations of *NaP* channels near the soma (Colbert and Johnston 1996). The *NaP* channels bring with them smaller but less expensive linear ranges.

It seems that linearization will always increase metabolic energy costs. However, the precise costs depend on the conductances used to amplify and/or attenuate successive synaptic inputs into a linear regime. Moreover, it also seems that longer ranges are more costly (compare Fig. 7(c) vs. Fig. 8(c) as mentioned in Section 3). Thus, an obvious prediction is that Nature is judicious in constructing linear ranges, using no more range than is needed at any point along the dendritic axis. In particular, as just noted above, smaller ranges will be used at more proximal locations and longer ranges more distally.

The linearizing conjecture is not the only possible reason for the *NaP* conductance. Vervaeke et al. (2006) conjecture, and supported with *in vitro* measurements, a role for *NaP* in controlling oscillatory responses of CA1 pyramidal neurons.

Our results in no way contradict this hypothesis. However, one is lead to wonder if both mechanisms can exist together. To answer the compatibility question requires a more sophisticated model than used here. Specifically, a more dynamic and accurate biophysical model needs to be used.

Such dynamic models, including more biophysical and anatomical details, will be investigated in further research. In addition, such models will also provide a platform to re-evaluate the steady-state assumption here and to determine the effective range of its validity relative to neuronal time constants.

From a larger perspective, our goal is to understand the evolved biophysics of neurons through the lens of constrained optimizations. A most promising set of constraints combines information and metabolic energy calculations. For example, these measurements of information rate and energy rate can be combined to form time-independent ratios with units that are directly proportional to bits-per-joule, or equivalently, through a constant, bits-per-mole-of-ATP. In this regard the results here will be of substantial relevance. Indeed, if future calculations of dendritic information costs are as parametrically sensitive as previous ones (e.g., see the rather flat, but concave function that is maximized in Levy and Baxter 1996), even small energy differences, such as shown in Fig. 6 comparing the passive model to I_{NaP} models, will matter.

Linearization of dendritic excitation is an important part of this optimization approach. When extracting information, the Bayesian approach is optimal because it is, up to equivalence, the only approach that is fully and logically consistent as well as neurally plausible under one particular approach. That approach is the use of sufficient statistics of fixed dimension (ideas discussed in Levy et al. 1990 and further elaborated on in Levy and Morel 2006). Such statistics maintain a relatively low dimension (e.g., unidimensional corresponding to a neuron's somatic depolarization) and are guaranteed to use *all* available information. In the same vein, it is important to realize, even without a calculation but dependent on theorems of statistical probability theory (Bernando and Smith 2000), that such a guarantee is itself an optimization! More to the point here, it is also known that sufficient statistics of fixed dimension can only be built by linear summation, and such statistics are equivalent in information to the predicted probability distribution itself.

Simple optimizations (calculations not shown) using the data here fail to produce interesting results. Essentially very low, non-physiological rates of excitation produce the most bits/joule. Apparently to use the data here to produce a sensible bits/joule optimization of dendritic function will require further considerations. These considerations include a prior probability distribution and various potential sources of randomness, e.g., failure rates, variability of individual synaptic events, and band-limited thermal noise. Nevertheless, without the data here, the justification of such calculation and the assumed range of the postsynaptic excitation variable would be substantially weakened.

In conclusion, as recognized by Bernander et al. (1994), it is a curious fact that microscopic complexity in Nature can lead to theoretical simplicity. Here we have investigated the specific examples where the great complexity inherent in channels whose net conductance depends on nonlinear activation and inactivation curves can be used to linearize a particular dendritic computation.

This approach, and others like it, will lead to the appropriate functional interpretations that make sense of the zoo of voltage-dependent channels found in dendrites. Each sufficiently well developed perspective of dendritic function will bring with it sufficient constraints for experimental tests. That is, with the appropriate set of constraints, we can anticipate strong, testable hypotheses from each biophysical model. Of course there will not be one universally correct dendritic model: dendrites of different cell types will perform different functions; different dendrites on the same cell will perform different functions; and it even seems likely that the same dendrite might perform different functions depending on variables such as stage of awakeness, sleep, or attentional considerations.

Acknowledgements The authors would like to thank the Walter and Mary Munster Foundation for their support.

Appendix A

The relationships of Table 5 are made more transparent by a few equations. Using the *NaP*-enhanced system as an example, the basic current equations (d = dendrite, s = synapses, and NaP = persistent sodium) and their derivatives are

$$
\begin{aligned}
&I_d = g_d(V_m(g_s) - V_d), \quad \frac{dI_d}{dg_s} = g_d \frac{dV_m}{dg_s},\\
&I_s = g_s(V_m(g_s) - V_s), \quad \frac{dI_s}{dg_s} = V_m(g_s) - V_s + g_d \frac{dV_m}{dg_s},\\
&I_{NaP} = \overline{g}_{NaP}(V_m)\left(V_m(g_s) - V_{\mathrm{Na}}^{\mathrm{Nernst}}\right)\\
&\qquad = \overline{g}_{NaP} f(V_m)\left(V_m(g_s) - V_{\mathrm{Na}}^{\mathrm{Nernst}}\right)\\
&\frac{dI_{NaP}}{dg_s} = \overline{g}_{NaP}\left(V_m(g_s) - V_{\mathrm{Na}}^{\mathrm{Nernst}}\right)\frac{df(V_m)}{dV_m}\frac{dV_m}{dg_s} + \overline{g}_{NaP} f(V_m)\frac{dV_m}{dg_s}.
\end{aligned}
$$

Remembering that, in steady-state, the sum of the currents is zero (i.e., $I_s+I_{NaP}+I_d=0$), the derivatives can also be combined and $\frac{df(V_m)}{dV_m}$ solved for such that

$$\frac{df(V_m)}{dV_m} = -\left[\frac{g_d\frac{dV_m}{dg_s} + V_m(g_s) - V_s + g_s\frac{dV_m}{dg_s} + \overline{g}_{NaP}f(V_m)\frac{dV_m}{dg_s}}{\overline{g}_{NaP}\left(V_m(g_s) - V_{\mathrm{Na}}^{\mathrm{Nernst}}\right)\frac{dV_m}{dg_s}}\right] \tag{9}$$

Let $V_s=0$ and, in the linear range, let $\frac{dV_m(g_s)}{dg_s}$ = constant = K. Rearranging Eq. (9) gives

$$\frac{df(V_m)}{dV_m}\overline{g}_{NaP}\left(V_m(g_s) - V_{\mathrm{Na}}^{\mathrm{Nernst}}\right)K = -[g_dK + V_m(g_s) + g_sK + \overline{g}_{NaP}f(V_m)K].$$

Taking the derivative with respect to V_m of both sides of this equation sets up the ordinary differential equation

$$\frac{d^2f(V_m)}{dV_m^2}\left(V_m(g_s) - V_{\mathrm{Na}}^{\mathrm{Nernst}}\right) + 2\frac{df(V_m)}{dV_m} + \frac{2}{\overline{g}_{NaP}K} = 0,$$

which can be solved for $f(V_m)$. That is,

$$f(V_m) = -\frac{1}{\overline{g}_{Nap}K}\left[V_m(g_s) + \frac{C_1\overline{g}_{NaP}K + \left(V_{\mathrm{Na}}^{\mathrm{Nernst}}\right)^2}{V_m(g_s) - V_{\mathrm{Na}}^{\mathrm{Nernst}}}\right] + C_2, \tag{10}$$

where C_1 and C_2 are constants. Finally, Eq. (10) and its derivative $df(V_m)/dV_m$ can be substituted back into Eq. (9) which can then be solved for V_m in the linear range.

$$V_m = V_{\mathrm{Na}}^{\mathrm{Nernst}} + (g_d + g_s + C_2\overline{g}_{NaP})K \text{ or, equivalently,}$$

$$K = \left|\frac{dV_m}{dg_s}\right|_{\mathrm{cst}} = \frac{V_m(g_s) - V_{\mathrm{Na}}^{\mathrm{Nernst}}}{g_d + g_s + C_2\overline{g}_{NaP}},$$

where C_2 is a constant whose value is independent of g_s and V_m. The last equation shows that, in the linear range, since V_m changes linearly with g_s, the numerator is a linear function of g_s. This implies that the denominator also changes linearly (i.e., if g_s is doubled so must g_d and $\overline{g}_{NaP}$) to maintain $dV_m(g_s)/dg_s$ = constant. The inverse relationship between $dV_m(g_s)/dg_s$ and g_d or g_s or $\overline{g}_{NaP}$ is also apparent in the last equation. Equivalent equations can be derived for a system which includes I_A.

Appendix B

Table 6 Parameters of active dendritic conductances

		Activation		Inactivation		
		$V_{1/2}$	k	$V_{1/2}$	k	
Persistent Sodium						
Agrawal et al. 2001		−37.6 mV	7.4 mV			EC layer V, soma
Magistretti and Alonso 1999				−48.8 mV	−10 mV	EC layer II, soma
French et al., 1990		−49 mV	5 mV	−49 mV	−9 mV	CA1, soma
A-type Potassium						
Hoffman et al. 1997:	<100 μm	11 mV	18 mV	−56 mV	−8 mV	CA1
	>100 μm	−1 mV	15 mV	−56 mV	−8 mV	V_{rev}=−80 mV
Bekkers 2000:	<250 μm	−24.5 mV	16.9 mV	−72.3 mV	5.9 mV	Neocortex layer V
	>250 μm	−22.9 mV	16.2 mV	−83.1 mV	6.5 mV	V_{rev}=−66 mV

References

Agrawal, N., Hamam, B. N., Magistretti, J., Alonso, A., & Ragsdale, D. S. (2001). Persistent sodium channel activity mediates subthreshold membrane potential oscillations and low-threshold spikes in rat entorhinal cortex layer v neurons. *Neuroscience*, *102*, 53–64. doi:10.1016/S0306-4522(00)00455-3.

Andrasfalvy, B. K., & Magee, J. C. (2001). Distance-dependent increase in AMPA receptor number in the dendrites of adult hippocampal CA1 pyramidal neurons. *The Journal of Neuroscience*, *21*, 9151–9159.

Attwell, D., & Gibb, A. (2005). Neuroenergetics and the kinetic design of excitatory synapses. *Nature Reviews. Neuroscience*, *11*, 841–849. doi:10.1038/nrn1784.

Attwell, D., & Laughlin, S. B. (2001). An energy budget for signalling in the grey matter of the brain. *Journal of Cerebral Blood Flow and Metabolism*, *21*, 1133–1145. doi:10.1097/00004647-200110000-00001.

Balasubramanian, V., & Berry II, M. J. (2002). A test of metabolically efficient coding in the retina. *Network*, *13*, 531–552.

Bekkers, J. M. (2000). Distribution and activation of voltage-gated potassium channels in cell-attached and outside-out patches from large layer 5 cortical pyramidal neurons of the rat. *The Journal of Physiology*, *525*, 611–620. doi:10.1111/j.1469-7793.2000.t01-2-00611.x.

Bernander, O., Koch, C., & Douglas, R. J. (1994). Amplification and linearization of distal synaptic input to cortical pyramidal cells. *Journal of Neurophysiology*, *72*, 2743–2753.

Bernardo, J. M., & Smith, A. F. M. (2000). *Bayesian theory*. New York: Wiley 608 pp.

Carandini, M., Heeger, D. J., & Movshon, J. A. (1997). Linearity and normalization in simple cells of the macaque primary visual cortex. *The Journal of Neuroscience*, *17*, 8621–8644.

Cash, S., & Yuste, R. (1999). Linear summation of excitatory inputs by CA1 pyramidal neurons. *Neuron*, *22*, 383–394. doi:10.1016/S0896-6273(00)81098-3.

Colbert, C. M., & Johnston, D. (1996). Axonal action-potential initiation and Na+ channel densities in the soma and axon initial segment of subicular pyramidal neurons. *The Journal of Neuroscience*, *16*, 6676–6686.

Cook, E. P., Wilhelm, A. C., Guest, J. A., Lian, Y., Masse, N. Y., & Colbert, C. M. (2007). The neuronal transfer function: contributions from voltage- and time-dependent mechanisms. *Progress in Brain Research*, *165*, 1–11. doi:10.1016/S0079-6123(06)65001-2.

Crochet, S., & Petersen, C. C. H. (2006). Correlating whisker behavior with membrane potential in barrel cortex of awake mice. *Nature Neuroscience*, *9*, 608–610. doi:10.1038/nn1690.

DeAngelis, G. C., Ohzawa, I., & Freeman, R. D. (1993). Spatiotemporal organization of simple-cell receptive fields in the cat's striate cortex. II. Linearity of temporal and spatial summation. *Journal of Neurophysiology*, *69*, 1118–1135.

Destexhe, A., Rudolph, M., & Pare, D. (2003). The high-conductance state of neocortical neurons *in vivo*. *Nature Reviews. Neuroscience*, *4*, 739–751. doi:10.1038/nrn1198.

Fee, M. S. (2000). Active stabilization of electrodes for intracellular recording in awake behaving animals. *Neuron*, *27*, 461–468. doi:10.1016/S0896-6273(00)00057-X.

Ferster, D. (1994). Linearity of synaptic interactions in the assembly of receptive fields in cat visual cortex. *Current Opinion in Neurobiology*, *4*, 563–568. doi:10.1016/0959-4388(94)90058-2.

French, C. R., Sah, P., Buckett, K. J., & Gage, P. W. (1990). A voltage-dependent persistent sodium current in mammalian hippocampal neurons. *The Journal of General Physiology*, *95*, 1139–1157. doi:10.1085/jgp.95.6.1139.

Gasparini, S., & Magee, J. C. (2006). State-dependent dendritic computation in hippocampal ca1 pyramidal neurons. *The Journal of Neuroscience*, *26*, 2088–2100. doi:10.1523/JNEUROSCI.4428-05.2006.

Goldberg, D. H., Sripati, A. P., & Andreou, A. G. (2003). Energy efficiency in a channel model for the spiking axon. Neurocomputing 52–54. *Computational Neuroscience: Trends in Research*, *2003*, 39–44.

Goldman, D. E. (1943). Potential, impedance and rectification in membranes. *The Journal of General Physiology*, *27*, 37–60. doi:10.1085/jgp.27.1.37.

Gulledge, A. T., Kampa, B. M., & Stuart, G. J. (2005). Synaptic integration in dendritic trees. *Journal of Neurobiology*, *64*, 75–90. doi:10.1002/neu.20144.

Hasenstaub, A., Shu, Y., Haider, B., Kraushaar, U., Duque, A., & McCormick, D. A. (2005). Inhibitory postsynaptic potentials carry synchronized frequency information in active cortical networks. *Neuron*, *47*, 423–435. doi:10.1016/j.neuron.2005. 06.016.

Hodgkin, A. L., & Huxley, A. F. (1952). A quantitative description of membrane current and its application to conduction and excitation in nerve. *The Journal of Physiology*, *117*, 500–544.

Hodgkin, A. L., & Katz, B. (1949). The effect of sodium ions on the electrical activity of the giant axon of the squid. *The Journal of Physiology*, *108*, 37–77.

Hoffman, D. A., Magee, J. C., Colbert, C. M., & Johnston, D. (1997). K+ channel regulation of signal propagation in dendrites of hippocampal pyramidal neurons. *Nature*, *387*, 869–875. doi:10.1038/42571.

Jagadeesh, B., Wheat, H. S., & Ferster, D. (1993). Linearity of summation of synaptic potentials underlying direction selectivity in simple cells of the cat visual cortex. *Science*, *262*, 1901–1904. doi:10.1126/science.8266083.

Johnston, D., Magee, J. C., Colbert, C. M., & Christie, B. R. (1996). Active properties of neuronal dendrites. *Annual Review of Neuroscience*, *19*, 165–186. doi:10.1146/annurev.ne.19.030196.001121.

Laughlin, S. B., & Sejnowski, T. J. (2003). Communication in neural networks. *Science*, *301*, 1870–1874. doi:10.1126/science.1089662.

Léger, J.-F., Stern, E. A., Aertsen, A., & Heck, D. (2005). Synaptic integration in rat frontal cortex shaped by network activity. *Journal of Neurophysiology*, *93*, 281–293. doi:10.1152/jn.00067.2003.

Levy, W. B., & Baxter, R. A. (1996). Energy efficient neural codes. *Neural Computation*, *8*, 531–543. doi:10.1162/neco.1996.8.3.531.

Levy, W. B., & Baxter, R. A. (2002). Energy-efficient neuronal computation via quantal synaptic failures. *The Journal of Neuroscience*, *22*, 4746–4755.

Levy, W. B with simulations by Morel, D. (2006). A Bayesian Constraint on Neural Computation. Proceeding of the IEEE, International Symposium on Information Theory (ISIT), Seattle, Washington, July 9–14.

Levy, W. B., Colbert, C. M., & Desmond, N. L. (1990). Elemental adaptive processes of neurons and synapses: a statistical/computational perspective. In M. Gluck & D. Rumelhart (Ed.) *Neuroscience and Connectionist Theory* (pp. 187–253). Lawrence Erlbaum Associates.

London, M., & Häusser, M. (2005). Dendritic computation. *Annual Review of Neuroscience*, *28*, 503–532.

Magee, J. C. (1998). Dendritic hyperpolarization-activated currents modify the integrative properties of hippocampal CA1 pyramidal neurons. *The Journal of Neuroscience*, *18*(19), 7613–7624.

Magee, J. C. (1999). Voltage-gated ion channels in dendrites. In G. Stuart, N. Spruston, & M. Häusser (Eds.), *Dendrites* (pp. 139–160). Oxford University Press.

Magee, J. C. (2000). Dendritic integration of excitatory synaptic input. *Nature Reviews. Neuroscience*, *1*, 181–190. doi:10.1038/35044552.

Magee, J. C., & Cook, E. P. (2000). Somatic EPSP amplitude of synapse location in hippocampal pyramidal neurons. *Nature Neuroscience*, *3*, 895–903. doi:10.1038/78800.

Magee, J. C., Hoffman, D., Colbert, C., & Johnston, D. (1998). Electrical and calcium signaling in dendrites of hippocampal pyramidal neurons. *Annual Review of Physiology*, *60*, 327–346. doi:10.1146/annurev.physiol.60.1.327.

Magistretti, J., & Alonso, A. (1999). Biophysical properties and slow voltage-dependent inactivation of a sustained sodium current in entorhinal cortex layer-II principal neurons. *The Journal of General Physiology*, *114*, 491–509. doi:10.1085/jgp.114.4.491.

McCulloch, W. S., & Pitts, W. H. (1943). A logical calculus of the ideas immanent in nervous activity. *The Bulletin of Mathematical Biophysics*, *5*, 115–133. doi:10.1007/BF02478259.

Morel, D., & Levy, W. B. (2007). Persistent sodium is a better linearizing mechanism than the hyperpolarization-activated current. *Neurocomputing*, *70*, 1635–1639. doi:10.1016/j.neucom.2006.10.054.

Paré, D., Shink, E., Gaudreau, H., Destexhe, A., & Lang, E. J. (1998). Impact of spontaneous synaptic activity on the resting properties of cat neocortical pyramidal neurons *in vivo*. *Journal of Neurophysiology*, *79*, 1450–1460.

Polsky, A., Mel, B. W., & Schiller, J. (2004). Computational subunits in thin dendrites of pyramidal cells. *Nature Neuroscience*, *7*, 621–627. doi:10.1038/nn1253.

Priebe, J., & Ferster, D. (2005). Direction selectivity of excitation and inhibition in simple cells of the cat primary visual cortex. *Neuron*, *45*, 133–145. doi:10.1016/j.neuron.2004.12.024.

Sarpeshkar, R. (1998). Analog versus digital: extrapolating from electronics to neurobiology. *Neural Computation*, *10*, 1601–1638. doi:10.1162/089976698300017052.

Spruston, N., Jonas, P., & Sakmann, B. (1995). Dendritic glutamate receptor channels in rat hippocampal CA3 and CA1 pyramidal neurons. *The Journal of Physiology*, *482*, 325–352.

Steriade, M., Timofeev, I., & Grenier, F. (2001). Natural waking and sleep states: a view from inside neocortical neurons. *Journal of Neurophysiology*, *85*, 1969–1985.

Vervaeke, K., Hu, H., Graham, L. J., & Storm, J. F. (2006). Contrasting effects of the persistent Na+ current on neuronal excitability and spike timing. *Neuron*, *49*, 257–270. doi:10.1016/j.neuron.2005.12.022.

Vincent, T. V., & Baddeley, R. J. (2003). Synaptic energy efficiency in retinal processing. *Vision Research*, *43*, 1283–1290. doi:10.1016/S0042-6989(03)00096-8.

Vincent, T. V., Baddeley, R. J., Troscianko, T., & Gilchrist, I. D. (2005). Is the early visual system optimized to be energy efficient? *Network*, *16*, 175–190.

Yuste, R., & Tank, D. W. (1996). Dendritic integration in mammalian neurons a century after Cajal. *Neuron*, *16*, 701–716. doi:10.1016/S0896-6273(00)80091-4.